01 Aug 2019

Fabrication and Characterization of $Al_xCrCuFeNi_2$ High-Entropy Alloys Coatings by Laser Metal Deposition

Wenyuan Cui

Xinchang Zhang

Lan Li

Yitao Chen

et. al. For a complete list of authors, see https://scholarsmine.mst.edu/mec_aereng_facwork/4475

Recommended Citation

W. Cui et al., "Fabrication and Characterization of $Al_xCrCuFeNi_2$ High-Entropy Alloys Coatings by Laser Metal Deposition," *Procedia Manufacturing*, vol. 39, pp. 509-518, Elsevier B.V., Aug 2019.
The definitive version is available at https://doi.org/10.1016/j.promfg.2020.01.408

Available online at www.sciencedirect.com

ScienceDirect

Procedia Manufacturing 39 (2019) 509–518

Procedia MANUFACTURING

www.elsevier.com/locate/procedia

25th International Conference on Production Research Manufacturing Innovation: Cyber Physical Manufacturing
August 9-14, 2019 | Chicago, Illinois (USA)

Fabrication and Characterization of $Al_xCrCuFeNi_2$ High-Entropy Alloys Coatings by Laser Metal Deposition

Wenyuan Cui[a,*], Xinchang Zhang[a], Lan Li[a], Yitao Chen[a], Tan Pan[a], Frank Liou [a]

[a] *Department of Mechanical and Aerospace Engineering, Missouri Univesity of Science and Technology, Rolla, MO, 65409, United States*

Abstract

High-entropy alloys (HEAs) are becoming new hot spots in the metallic materials community, which are defined to contain equiatomic or close-to-equiatomic compositions. HEAs can possess many interesting mechanical properties, and in particular, they have the great potential to be used as coating materials requiring high hardness and wear resistance. In this study, the feasibility of fabrication $Al_xCrCuFeNi_2$ (x=0,0.75) HEAs was investigated via laser metal deposition from elemental powders. The microstructure, phase structure, and hardness were studied by an optical microscope, scanning electron microscopy with energy dispersive spectroscopy (SEM/EDS), electron backscatter diffraction (EBSD) and Vickers hardness tester. The bonding between the $Al_xCrCuFeNi_2$ (x = 0,0.75) HEAs and AISI 304 stainless steel were good combinations. The $Al_{0.75}CrCrFeNi_2$ alloy consisted of columnar dendritic microstructure with Al/Ni enrichment in the dendritic regions. The phase structure of the $Al_xCrCuFeNi_2$ (x = 0,0.75) HEAs were face center cubic structure as identified by EBSD. Vickers hardness results indicate that the average hardness of $CrCuFeNi_2$ HEA was 175 HV. With the addition of aluminium, the Vickers hardness of $Al_{0.75}CrCuFeNi_2$ HEA increased to 285 HV.

Keywords: High-entropy alloys; additive manufacturing; laser metal deposition; microstructure; elemental powder

* Corresponding author. Tel.:+1-865-898-8963.
E-mail address: wcz68@mst.edu

2351-9789
10.1016/j.promfg.2020.01.408

1. Introduction

Conventional metallurgical theory suggests that the multiple alloying elements in an alloy may result in the formation of complex compounds. Recently this paradigm has been broken by high-entropy alloys (HEAs) developed by Yeh et al.[1] HEAs are composed of five or more principle elements in equimolar or near-equimolar ratios. The high mixing entropy of multi-principle elements induces the formation of solid-solution structure, e.g., face center cubic (FCC) or body center cubic (BCC) or FCC combined with BCC [1–6]. The discovery of HEAs has brought a new alloy design concept and generated researchers' interest in the past decade. An AlCrFeCoNi HEA was prepared by vacuum arc melting and exhibited excellent compressive strength 2004.23 MPa [2]. Another study of $AlCrFeCuNi_x$ ($0.6 \leq x \leq 1.4$) HEAs was prepared by casting reported by Jinhong et al., which found the hardness of as-cast HEAs decreased as x increased from 1.0 to 1.4 [3]. Dong et al. investigated the $AlCrFeNiMo_x$ (x = 0,0.2,0.5,0.8 and 1.0 in molar ratios) HEAs produced by vacuum melting [7]. Their work showed $AlCrFeNiMo_{0.2}$ HEA possessed good fracture strength of 3222 MPa and plastic strain of 0.287, which implies its potential application in industrial areas. These HEAs were fabricated by casting or vacuum melting. Unlike the previous studies, this work will implement the laser metal deposition (LMD) method to fabricate the $Al_xCrCuFeNi_2$ (x = 0, 0.75 in molar ratios) HEAs.

As an advanced additive manufacturing technology, LMD can accomplish layer-by-layer fabrication of near net-shaped components by introducing a powder stream through a high energy laser beam [4,5,8–10]. A melt pool is formed by rastering the laser beam, and the powders are injected into the melt pool to deposit each layer during the LMD process. Layer by layer composition changes, the introduction of a dissimilar metal interlayer and control over the melt zone size can be accommodated [4,9–13]. A FeCoNiCrCu HEA coating was synthesized, and its microhardness reached 375 $HV_{0.5}$, which was about 50% higher than that of the same alloy prepared by arc melting [4]. With the additional of titanium content, $Al_2CrFeNiCoCuTi_x$ (x = 0, 0.5, 1.0, 1.5 and 2.0 in molar ratios) HEAs showed good corrosion and wear resistance on Q235 steel substrate [10]. Few research has been devoted to the fabrication of $AlCrCuFeNi_2$ HEAs by LMD.

In this paper, the feasibility of fabrication $Al_xCrCuFeNi_2$ (x = 0, 0.75 in molar ratios) HEA coatings on AISI 304 stainless steel (SS) was performed by laser metal deposition technology using elemental powders. The metallurgical bonding, microstructure, and Vickers hardness were investigated.

2. Experimental

2.1. LMD processing

Gas-atomized elemental powders of aluminium (Al), chromium (Cr), copper (Cu), iron (Fe) and nickel (Ni) purchased from Atlantic Equipment Engineers Inc. was used as precursor materials. The particle size of the elemental powders provided by Atlantic Equipment Inc. is as tabulated in Table 1. The elemental powders were weighted in the required ratios and then mixed by a Turbula mixer (Glen Mills Inc., Clifton, NJ, USA) for 30 mins to obtain homogeneous blends. Elemental compositions (atomic %) of the as-blended HEAs are given in Table 2.

Table 1. Particle size distribution of the elemental powders.

Materials	US Standard Mesh
Al	-100
Cr	-100
Cu	-100
Fe	-100
Ni	-100/+325

Table 2. Nominal compositions (atomic %) of HEAs.

Alloys	Al	Cr	Cu	Fe	Ni
$CrCuFeNi_2$	0	20	20	20	40
$Al_{0.75}CrCuFeNi_2$	13	17	17	17	36

The schematic of the LMD system is shown in Figure 1. The 1 kW continuous-wave YAG fiber laser (IPG, Photonics, Oxford, MA, USA) was used as a heat source with a beam diameter of 2 mm. The metallic powders were fed through a vibration X2 powder feed system (Powder Motion Labs, MO, USA). The powders were introduced into the melt pool by an alumina tube. Argon gas was used as a carrier gas to deliver the powder mixtures to the melt pool. The movement during the laser deposition was achieved through a computer numerical control (CNC) table.

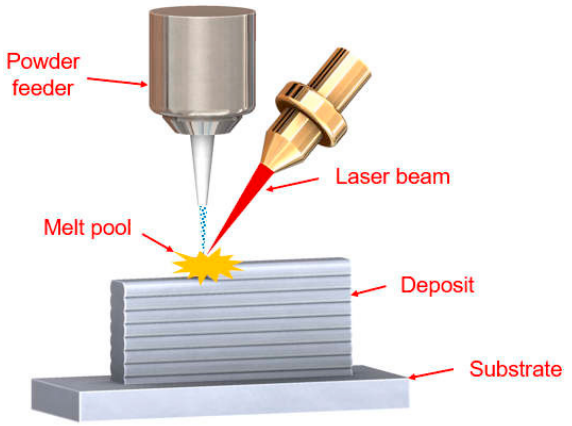

Fig. 1. Schematic of the laser metal deposition (LMD) system.

Commercially procured AISI 304 SS bar stock (dimension: 2 inch × 2 inch × 0.25 inch) was used as the substrate and cleaned with acetone to clean the surface. A preheating scan was performed by running the laser across the substrate. The thin wall structure was built, and the laser power of the initial three layers was conducted at 700 W and 8.5% (3.36 g/min) powder feed rate. The remaining of the deposition was carried out at 600 W and 8.5% (3.36 g/min) powder feed rate with 1 mm layer thickness.

2.2. Characterization

For microstructural characterization, the deposits were transverse cross-sectioned and prepared with standard metallographic methods. The samples were polished with 320-1200 grit SiC grinding paper, and the final mechanical polish was 0.05 µm silica suspension. The specimens were given the electrolytic etching in the nitric acid solution (70 mL nitric acid and 30 mL distilled water).

A Hirox optical microscope investigated the $Al_xCrCuFeNi_2$ HEAs morphology. The scanning electron microscopy (SEM), elemental analysis using energy dispersive spectroscopy (EDS), and electron backscatter diffraction (EBSD) studies of the specimens were carried out in a Helios Nanolab 600 SEM coupled with an EDS and an EBSD detector. The obtained EBSD data was processed and analyzed using Aztec software. The hardness was obtained with a Struers Duramin hardness tester (Struers Inc., Cleveland, OH, USA) using a 9.81 N force and 10 s load duration.

3. Results and discussion

3.1. Microstructure

Figure 2 shows the optical images of the deposited HEAs. The deposit was shown in the top area in Figure 2a while the bottom part was AISI 304 SS substrate. An explicit interface was seen between the deposit and the AISI 304 SS substrate. The columnar dendrite microstructure was observed from Figure 2b. Similarly, a good metallurgical bonding existed between $Al_{0.75}CrCuFeNi_2$ HEA and the AISI 304 SS substrate. The dendritic continued in $Al_{0.75}CrCuFeNi_2$ alloy. The growth direction of these columnar was identified to be along with the deposition direction, which could be correlated with the solidification direction during the LMD process.

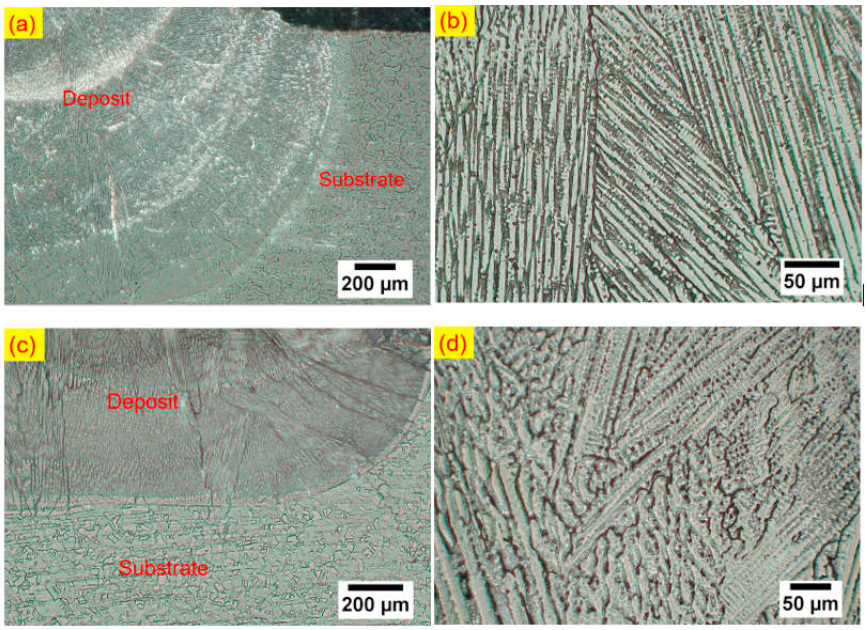

Fig. 2. Optical images of (a) the interface between $CrCuFeNi_2$ HEA and AISI 304 SS substrate, (b) microstructure of $CrCuFeNi_2$ HEA, (c) the interface between $Al_{0.75}CrCuFeNi_2$ HEA and AISI 304 SS substrate and (d) microstructure of $Al_{0.75}CrCuFeNi_2$ HEA.

3.2. EDS and EBSD analysis

The evolution in chemistry from the substrate to the $CrCuFeNi_2$ HEA was characterized by EDS line scan first. The quantitative results are plotted in Figure 3a. The results measured by EDS of the AISI 304 SS substrate (Cr: ~18-19 atomic %, Fe: ~70-71 atomic %, Ni: ~9-10 atomic % in Figure 3a) did not derive from the nominal AISI 304 SS chemical compositions. Mn (~ 1-2 atomic %) was detected by EDS in AISI 304 SS substrate but was not shown in Figure 3. The elemental compositions of Cu (~18-21 atomic %) and Ni (~35-38 atomic %) increased while that of Fe (~23-26 atomic %) reduced, and Cr (~20 atomic %) remained changed from the substrate to the $CrCuFeNi_2$ HEA deposit. A small amount of Cu (~1-2 atomic %) was detected in the substrate because the substrate was mixed with the HEA deposit. The distribution of the consisted compositions from the substrate to the $Al_{0.75}CrCuFeNi_2$ HEA was shown in Figure 3b. The constituents of the $Al_{0.75}CrCuFeNi_2$ HEA were determined by EDS (Al: ~9-10 atomic %, Cr: ~19 atomic %, Cu: ~17 atomic %, Fe: ~20 atomic %, Ni: ~ 32-34 atomic %). The difference between the as-blended (13 atomic %) and as-deposited aluminium (~9-10 atomic %) compositions could be attributed to the inconsistency of powder capture efficiency and evaporation due to its low melting point.

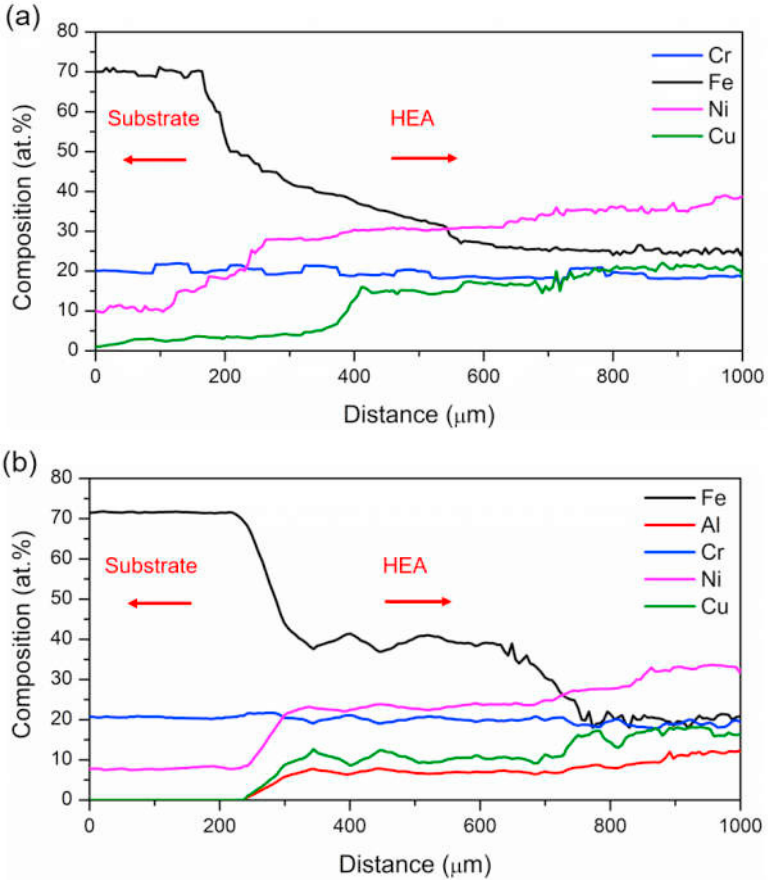

Fig. 3. Elemental composition evolution (a) the interface between AISI 304 SS substrate and $CrCuFeNi_2$ HEA, (b) the interface from AISI 304 SS substrate to $Al_{0.75}CrCuFeNi_2$ HEA.

EBSD and EDS measurements were conducted in the aim of differentiating structure and phase information of the $Al_xCrCuFeNi_2$ (x = 0, 0.75) alloys. Regions of interest and phase analysis of $CrCuFeNi_2$ and $Al_{0.75}CrCuFeNi_2$ alloys are shown in Figures 4 and 5 respectively. Figures 4 and 5 indicate an FCC structure in both HEA fabrications. The phase fractions and the corresponding lattice parameter identified by EBSD are listed in Table 3. The zero solution is the fraction of the selected area whose crystal structure could not be solved by the software.

Table 3 Summary of the lattice parameter and phase fraction (%) of the $Al_xCrCuFeNi_2$ HEAs obtained from EBSD analysis.

Alloy	Phase Name	Space Group	Lattice Parameter (Å)	Fraction (%)
$CrCuFeNi_2$	FCC	Fm-3m (225)	3.66	88.2
	BCC	Im-3m (229)	2.93	0.13
	Zero solution	-	-	11.67
$Al_{0.75}CrCuFeNi_2$	FCC	Fm-3m (225)	3.66	99.3
	BCC	Im-3m (229)	2.93	0.09
	Zero solution	-	-	0.61

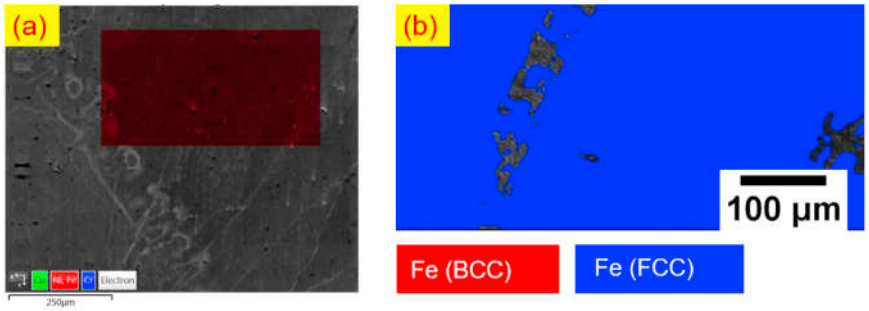

Fig.4. EBSD phase map indicates predominating FCC phase in the $CrCuFeNi_2$ alloy. (a) The region of interest on $CrCrFeNi_2$ alloy (b) Phase map shows predominantly FCC phase (represented by blue color) within the region of interest.

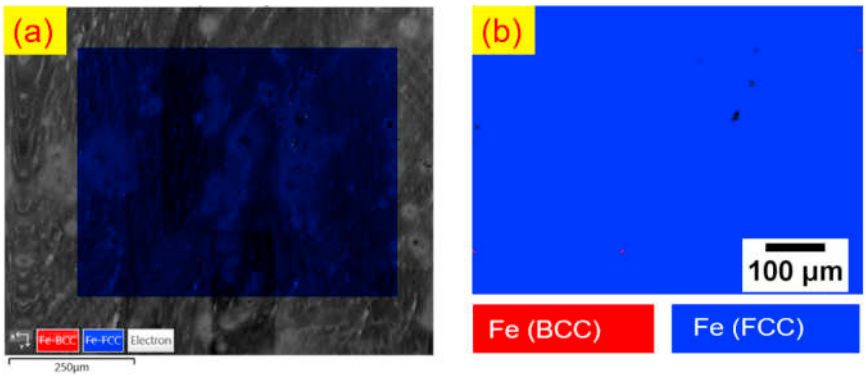

Fig.5. EBSD phase map indicates predominating FCC phase in the $Al_{0.75}CrCuFeNi_2$ alloy. (a) The region of interest on $Al_{0.75}CrCuFeNi_2$ alloy, (b) Phase map shows predominantly FCC phase (represented by blue color) within the region of interest.

Figures 6 and 7 show the EDS element maps obtained from the $Al_xCrCuFeNi_2$ HEAs. The Fe-Kα, Cr-Kα, Ni-Kα, Cu-Kα and Al-Kα signals were used to estimate the elemental compositions within the regions of interest in the deposits. EDS elemental compositions were gathered from the dendritic microstructures for the $Al_xCrCuFeNi_2$ (x = 0, 0.75) HEAs. The standardless measurements are listed in Table 4. The microstructure of $CrCuFeNi_2$ alloy exhibited a dendritic microstructure as reported previously. Based on the previous EBSD phase analysis, this dendritic phase was likely to be a single FCC phase. While it was observed a distinct contrast between the dendritic and interdendritic regions (as seen in Figure 6), this contrast could be attributed to the segregation of Cu (which tended to partition and segregate readily [14,15]) as in Figure 6e. Table 4 shows that Cu was enriched in the interdendritic regions. Figure 7 indicates that with the addition of aluminium, $Al_{0.75}CrCuFeNi_2$ alloy contained predominantly two phases. Associated with the results from Table 4, the dendritic phase was observed to be Al and Ni rich (Al+Ni: ~41 atomic %, Fe+Cr: ~18 atomic %), while the interdendritic microstructure was rich in Fe and Cr (Al+Ni: ~28 atomic %, Fe+Cr: ~52 atomic %). The Cu was deficient in the interdendritic regions.

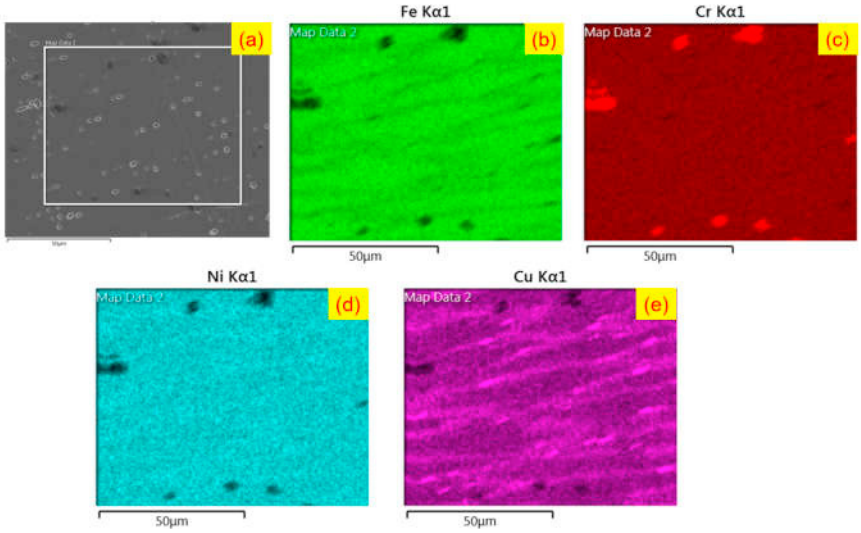

Fig.6. EDS elemental maps of $CrCuFeNi_2$ alloy, (a) region of interest, (b) element map of Fe, (c) element map of Cr, (d) element map of Ni and (e) element map of Cu.

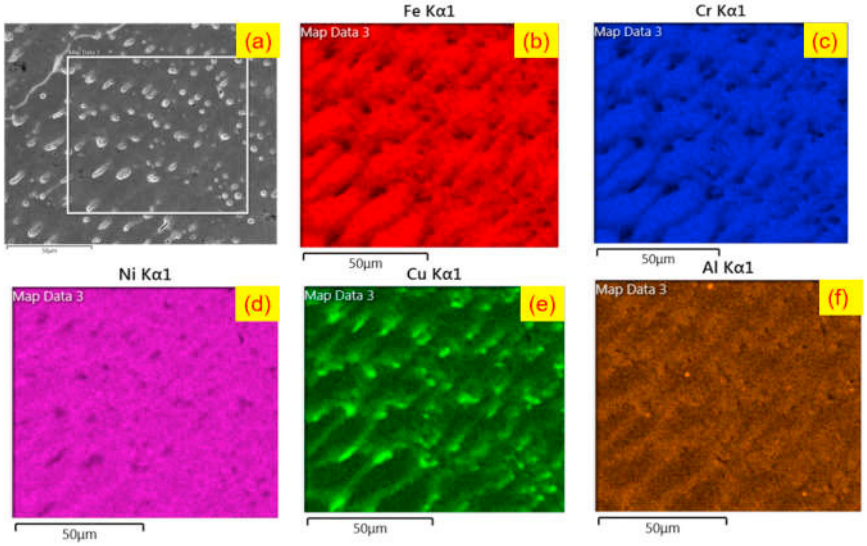

Fig.7. EDS elemental maps of $Al_{0.75}CrCuFeNi_2$ alloy, (a) region of interest, (b) element map of Fe, (c) element map of Cr, (d) element map of Ni, (e) element map of Cu and (f) element map of Al.

Table 4 Elemental compositions of the elements at different regions in atomic % for the $CrCuFeNi_2$ and $Al_{0.75}CrCrFeNi_2$ alloys.

Alloy	Area	Al	Cr	Cu	Fe	Ni
$CrCuFeNi_2$	Nominal	0	20	20	20	40
	Dendritic	0	18.5	18.7	27.1	35.7
	Interdendritic	0	16.9	25.9	21.4	35.8
$Al_{0.75}CrCuFeNi_2$	Nominal	13	17	17	17	36
	Dendritic	15	7.3	41.4	10.3	26
	Interdendritic	8	20	24	28	20

From the mixing enthalpy of atom-pair as listed in Table 5, it clearly shows that the mixing of enthalpy of Al and Ni is higher (-22 kJ/mol) than of other atom-pair. It indicates that Al and Ni atoms tend to form atom pairs and segregate. Similar results have been reported previously, with this microstructure being attributed to the spinodal decomposition [2,6,16–18].

Table 5 Mixing enthalpy of different atom-pair in the $CrCuFeNi_2$ and $Al_{0.75}CrCrFeNi_2$ alloys [19].

ΔHmix (kJ/mol)	Cu	Cr	Al	Ni
Fe	13	-1	-11	-2
Cu	-	12	-1	4
Cr	-	-	-10	-7
Al	-	-	-	-22

3.3. Vickers hardness

Figure 8 gives the Vickers hardness profiles of the $Al_xCrCuFeNi_2$ (x = 0, 0.75) alloys deposits on the AISI 304 SS substrates. The Vickers hardness of $CrCuFeNi_2$ alloy was around 175 HV, which could be attributed to the solid solution strengthening. Table 6 gives the Vickers hardness of various alloys, including AISI 304 SS, Inconel 625 and 7075-T6 aluminium [20,21], and $Al_{0.75}CrCuFeNi_2$ alloy has the highest average hardness of 285 HV. With the addition of aluminium, the average Vickers hardness of $Al_{0.75}CrCuFeNi_2$ HEA reached 285 HV, because the second phase strengthening blocked the dislocation [6,18]. The high hardness of $Al_{0.75}CrCuFeNi_2$ HEA coating is expected to correlate with good performance in strength and wear resistance [10,13].

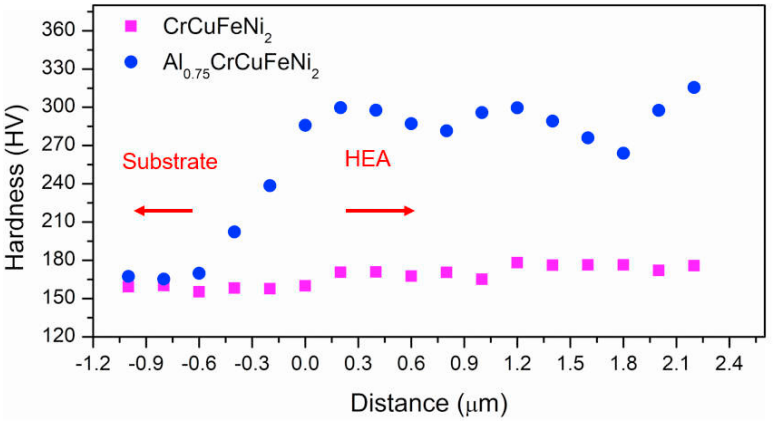

Figure 8 Vickers hardness profiles of the $Al_xCrCuFeNi_2$ (x = 0,0.75) alloys.

Table 6 Vickers hardness of various alloys.

Alloy	Hardness (HV)	Reference
$CrCuFeNi_2$	175	This work
$Al_{0.75}CrCuFeNi_2$	285	This work
AISI 304 SS	160	This work
Inconel 625	156	[21]
7075-T6 aluminium	118	[20]

4. Conclusions

$Al_xCrCuFeNi_2$ (x = 0,0.75 in molar ratios) HEAs were coated on AISI 304 stainless steel substrate via laser metal deposition technology. The metallurgical bonding, microstructure, and the Vickers hardness were investigated and discussed. The good metallurgical bonding was observed between the HEA coatings and the substrate. The $Al_xCrCuFeNi_2$ (x = 0,0.75) HEAs coating exhibited columnar dendritic microstructure and FCC structure identified by EBSD. $CrCuFeNi_2$ HEA was found to have an average hardness of 175 HV, while $Al_{0.75}CrCuFeNi_2$ HEA has a hardness of 285 HV.

Acknowledgments

The authors gratefully acknowledge the financial support from NSF (National Science Foundation) grants CMMI-1547042 and CMMI-1625736. The support from the Intelligent System Center (ISC) and Materials Research Center (MRC) at Missouri University of Science and Technology are also greatly appreciated.

References

[1] J.-W. Yeh, S.-K. Chen, S.-J. Lin, J.-Y. Gan, T.-S. Chin, T.-T. Shun, C.-H. Tsau, S.-Y. Chang, Nanostructured High-Entropy Alloys with Multiple Principal Elements: Novel Alloy Design Concepts and Outcomes, Adv. Eng. Mater. 6 (2004) 299–303. doi:10.1002/adem.200300567.

[2] Y.P. Wang, B.S. Li, M.X. Ren, C. Yang, H.Z. Fu, Microstructure and compressive properties of AlCrFeCoNi high entropy alloy, Mater. Sci. Eng. A. 491 (2008) 154–158. doi:10.1016/J.MSEA.2008.01.064.

[3] P. Jinhong, P. Ye, Z. Hui, Z. Lu, Microstructure and properties of AlCrFeCuNix (0.6 ≤ x ≤ 1.4) high-entropy alloys, Mater. Sci. Eng. A. 534 (2012) 228–233. doi:10.1016/J.MSEA.2011.11.063.

[4] H. Zhang, Y. Pan, Y.-Z. He, Synthesis and characterization of FeCoNiCrCu high-entropy alloy coating by laser cladding, Mater. Des. 32 (2011) 1910–1915. doi:10.1016/J.MATDES.2010.12.001.

[5] W. Cui, X. Zhang, F. Liou, Additive Manufacturing of High-Entropy Alloys - A Review, in: Proc. 28th Annu. Int. Solid Free. Fabr. Symp. – An Addit. Manuf. Conf., Austin, TX, 2017: pp. 712–724.

[6] W.-R. Wang, W.-L. Wang, S.-C. Wang, Y.-C. Tsai, C.-H. Lai, J.-W. Yeh, Effects of Al addition on the microstructure and mechanical property of AlxCoCrFeNi high-entropy alloys, Intermetallics. 26 (2012) 44–51. doi:10.1016/J.INTERMET.2012.03.005.

[7] Y. Dong, Y. Lu, J. Kong, J. Zhang, T. Li, Microstructure and mechanical properties of multi-component AlCrFeNiMox high-entropy alloys, J. Alloys Compd. 573 (2013) 96–101. doi:10.1016/J.JALLCOM.2013.03.253.

[8] W. Li, A. Ghazanfari, D. McMillen, M.C. Leu, G.E. Hilmas, J. Watts, Fabricating ceramic components with water dissolvable support structures by the Ceramic On-Demand Extrusion process, CIRP Ann. 66 (2017) 225–228. doi:10.1016/J.CIRP.2017.04.129.

[9] A. Reichardt, R.P. Dillon, J.P. Borgonia, A.A. Shapiro, B.W. McEnerney, T. Momose, P. Hosemann, Development and characterization of Ti-6Al-4V to 304L stainless steel gradient components fabricated with laser deposition additive manufacturing, Mater. Des. 104 (2016) 404–413. doi:10.1016/J.MATDES.2016.05.016.

[10] X.W. Qiu, Y.P. Zhang, C.G. Liu, Effect of Ti content on structure and properties of Al2CrFeNiCoCuTix high-entropy alloy coatings, J. Alloys Compd. 585 (2014) 282–286. doi:10.1016/J.JALLCOM.2013.09.083.

[11] W. Cui, S. Karnati, X. Zhang, E. Burns, F. Liou, Fabrication of AlCoCrFeNi High-Entropy Alloy Coating on an AISI 304 Substrate via

a CoFe2Ni Intermediate Layer, Entropy. 21 (2019) 2. doi:10.3390/e21010002.

[12] W. Li, A.J. Martin, B. Kroehler, A. Henderson, T. Huang, J. Watts, G.E. Hilmas, M.C. Leu, Fabricating Functionally Graded Materials by Ceramic On-Demand Extrusion with Dynamic Mixing, in: Proc. 29th Annu. Int. Solid Free. Fabr. Symp. – An Addit. Manuf. Conf., Austin,TX,USA, 2018: pp. 1087–1099.

[13] S. Chen, Y. Tong, P. Liaw, S. Chen, Y. Tong, P.K. Liaw, Additive Manufacturing of High-Entropy Alloys: A Review, Entropy. 20 (2018) 937. doi:10.3390/e20120937.

[14] D. Choudhuri, T. Alam, T. Borkar, B. Gwalani, A.S. Mantri, S.G. Srinivasan, M.A. Gibson, R. Banerjee, Formation of a Huesler-like L21 phase in a CoCrCuFeNiAlTi high-entropy alloy, Scr. Mater. 100 (2015) 36–39. doi:10.1016/J.SCRIPTAMAT.2014.12.006.

[15] T. Borkar, B. Gwalani, D. Choudhuri, T. Alam, A.S. Mantri, M.A. Gibson, R. Banerjee, Hierarchical multi-scale microstructural evolution in an as-cast Al2CuCrFeNi2 complex concentrated alloy, Intermetallics. 71 (2016) 31–42. doi:10.1016/J.INTERMET.2015.12.013.

[16] S. Guo, C. Ng, C.T. Liu, Anomalous solidification microstructures in Co-free AlxCrCuFeNi2 high-entropy alloys, J. Alloys Compd. 557 (2013) 77–81. doi:10.1016/J.JALLCOM.2013.01.007.

[17] C. Ng, S. Guo, J. Luan, Q. Wang, J. Lu, S. Shi, C.T. Liu, Phase stability and tensile properties of Co-free Al0.5CrCuFeNi2 high-entropy alloys, J. Alloys Compd. 584 (2014) 530–537. doi:10.1016/J.JALLCOM.2013.09.105.

[18] Z. Tang, O.N. Senkov, C.M. Parish, C. Zhang, F. Zhang, L.J. Santodonato, G. Wang, G. Zhao, F. Yang, P.K. Liaw, Tensile ductility of an AlCoCrFeNi multi-phase high-entropy alloy through hot isostatic pressing (HIP) and homogenization, Mater. Sci. Eng. A. 647 (2015) 229–240. doi:10.1016/J.MSEA.2015.08.078.

[19] A. Takeuchi, A. Inoue, Classification of Bulk Metallic Glasses by Atomic Size Difference, Heat of Mixing and Period of Constituent Elements and Its Application to Characterization of the Main Alloying Element, Mater. Trans. 46 (2005) 2817–2829. doi:10.2320/matertrans.46.2817.

[20] A.S. El-Amoush, Intergranular corrosion behavior of the 7075-T6 aluminum alloy under different annealing conditions, Mater. Chem. Phys. 126 (2011) 607–613. doi:10.1016/J.MATCHEMPHYS.2011.01.010.

[21] M.A. Shaikh, M. Ahmad, K.A. Shoaib, J.I. Akhter, M. Iqbal, Precipitation hardening in Inconel * 625, Mater. Sci. Technol. 16 (2000) 129–132. doi:10.1179/026708300101507613.